

Near-infrared sideband generation induced by intense far-infrared radiation in GaAs quantum wells

J. Černe^{a)}

Department of Physics and Center for Terahertz Science and Technology, University of California, Santa Barbara, California 93106

J. Kono^{b)} and T. Inoshita

Quantum Transition Project, Japan Science and Technology Corporation, Tokyo 153, Japan

M. Sherwin

Department of Physics and Center for Terahertz Science and Technology, University of California, Santa Barbara, California 93106

M. Sundaram^{c)} and A. C. Gossard

Materials Department, University of California, Santa Barbara, California 93106

(Received 18 September 1996; accepted for publication 21 April 1997)

GaAs quantum wells are simultaneously illuminated with near-infrared (NIR) radiation at frequency ω_{nir} and intense far-infrared (FIR) radiation from a free-electron laser at ω_{fir} . Magnetic fields up to 9 T are applied. Strong and narrow sidebands are observed at $\omega_{\text{sideband}} = \omega_{\text{nir}} \pm 2\omega_{\text{fir}}$. The intensity of the sidebands is enhanced when either ω_{sideband} or ω_{nir} is near the onset of NIR absorption in the quantum well, or when ω_{fir} is near the free-electron cyclotron frequency. We attribute these sidebands to four-wave mixing of NIR and FIR photons whose energies differ by more than a factor of 100. © 1997 American Institute of Physics. [S0003-6951(97)00626-8]

Since far-infrared (FIR) radiation can couple very strongly to transitions in semiconductor quantum wells (QWs),¹ intense FIR radiation can lead to many interesting nonlinear effects in QWs including harmonic generation,^{2,3} saturation of intersubband transitions,⁴ ac Stark effect,^{5,6} resonant/nonresonant ionization of excitons,⁷ and quenching of photoluminescence (PL).^{8,9} The nonlinear interaction of FIR and near-infrared (NIR) radiation not only provides rich new physics, but also shows a strong potential for applications in a frequency regime which is underexploited technologically. For example, FIR-NIR mixing may have applications in modulating light at high frequencies, which is of central importance for optical communication. Further applications involve using NIR probes for fast, coherent detection of FIR radiation.¹⁰ This technique also could serve as a novel, nonlinear probe of FIR transitions in semiconductors. As is demonstrated in this letter, NIR-FIR mixing can dominate the optical emission of quantum heterostructures, so a greater understanding of this effect is crucial to a number of experimental and design scenarios.

Nondegenerate three- and four-wave mixing in semiconductors have been studied extensively in the NIR domain and in recent years these experiments have been extended to FIR frequencies. Most of these experiments involve generating weak FIR radiation by difference mixing two NIR lasers.^{11–13} Other experiments have mixed nondegenerate FIR photons.¹⁴ To our knowledge, no experiment to date has mixed intense FIR radiation with NIR radiation to produce NIR sidebands.

In this letter, low intensity NIR radiation, which is used to excite electron-hole pairs across the energy gap, mixes with high intensity FIR radiation to produce intense and narrow sidebands on either side of the NIR probe radiation. The frequency of the sideband radiation is:

$$\omega_{\text{sideband}} = \omega_{\text{nir}} \pm 2\omega_{\text{fir}},$$

where ω_{nir} and ω_{fir} are the NIR and FIR frequencies, respectively. The sideband intensity is doubly resonant in both the NIR and FIR, with resonant enhancement when ω_{nir} is tuned to the GaAs QW band edge, and when ω_{fir} approaches the free-electron cyclotron frequency.

The sample consisted of 50 undoped 100-Å-wide GaAs QWs between 150-Å-thick Al_{0.3}Ga_{0.7}As barriers. This multiple QW was grown by molecular beam epitaxy on a semi-insulating (100) GaAs substrate. A buffer layer consisting of 4000 Å GaAs and a smoothing superlattice were grown on top of the substrate.⁸

Great flexibility was achieved in this experiment by incorporating three continuously tunable parameters: FIR frequency, NIR frequency, and magnetic field B . University of California Santa Barbara's free-electron lasers (FELs) provide intense radiation (typically several hundred kW/cm² in this experiment) that can be continuously tuned from 4 to 160 cm⁻¹ (0.5–20 meV, 0.12–4.8 THz). As can be seen in Fig. 1, a cw Ti:sapphire laser (tunable NIR probe with photon energy of 1.1–1.8 eV) was used to create electron-hole pairs in the sample at 9 K. Simultaneously, FIR radiation with the electric field linearly polarized in the plane of the QW, and therefore not coupling to intersubband transitions, passed through the sample. The returning NIR radiation (consisting of reflected NIR laser, sidebands, and PL) was captured by 18 50-μm-diam optic fibers that surround a central excitation laser fiber. The NIR radiation was delivered to a double monochromator and a cooled GaAs photomultiplier tube. The output of the Ti:sapphire laser was modulated

^{a)}Present address: Dept. of Physics, University of Maryland, College Park, MD 20740; Electronic mail: jcerne@delphi.umd.edu

^{b)}Visiting scientist at the Center for Terahertz Science and Technology, University of California, Santa Barbara, CA.

^{c)}Present address: JPL, NASA, MS 302-231, 4800 Oak Grove Dr., Pasadena, CA 91109.

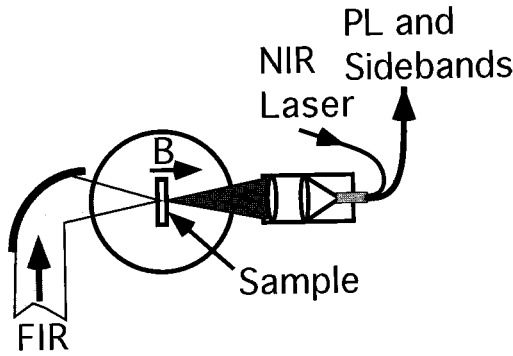


FIG. 1. A schematic of the experimental setup. NIR emission is detected during and after the FIR pulse has passed through the sample. The FIR radiation is polarized parallel to the plane of the QW.

acousto-optically to produce a $20 \mu\text{s}$ NIR excitation pulse that coincided with the $5 \mu\text{s}$ FIR pulse at the sample. Since the FIR pulse is much longer than any carrier relaxation time, the measurement is in steady-state. The change in NIR emission during the FIR pulse was due to carrier heating and sideband generation; no lattice heating was observed.⁹

Typical measurements involved fixing ω_{nir} and ω_{fir} at a constant B , and scanning the monochromator to measure PL and sidebands (see Fig. 2). The dependence of the sideband intensity on B was measured by tuning the NIR laser frequency to the $1s$ heavy hole (HH) exciton transition at each B , and scanning the monochromator to measure the $\omega_{\text{nir}} + 2\omega_{\text{fir}}$ sideband (see Fig. 3). The energy of the $1s$ HH exciton transition, $E_{\text{HH}}(B)$, followed the expected diamagnetic shift as a function of B .

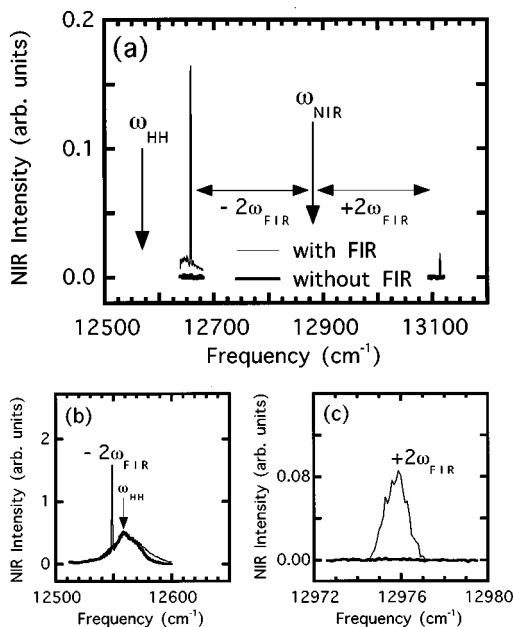


FIG. 2. Sidebands and PL observed at two FIR frequencies and three NIR frequencies at 8.5 T. (a) $\omega_{\text{fir}} = 115 \text{ cm}^{-1}$; $\omega_{\text{nir}} = 12888 \text{ cm}^{-1}$; (\pm) $\omega_{\text{sideband}} = 12658$ and 13118 cm^{-1} . The small, broad PL feature at 12650 cm^{-1} is a result of PL enhancement due to carrier heating. (b) $\omega_{\text{fir}} = 103 \text{ cm}^{-1}$; $\omega_{\text{nir}} = 12753 \text{ cm}^{-1}$; ($-$) $\omega_{\text{sideband}} = 12547 \text{ cm}^{-1}$. The high energy PL tail ($12560\text{--}12600 \text{ cm}^{-1}$) is slightly enhanced due to carrier heating. (c) $\omega_{\text{fir}} = 115 \text{ cm}^{-1}$; $\omega_{\text{nir}} = 12746 \text{ cm}^{-1}$; ($+$) $\omega_{\text{sideband}} = 12976 \text{ cm}^{-1}$. PL baseline is zero since the sideband is far above the PL emission peak.

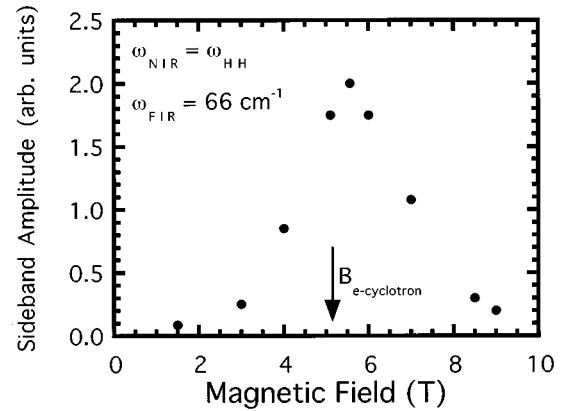


FIG. 3. Up-converted sideband amplitude as a function of magnetic field. The NIR excitation is tuned to the HH $1s$ exciton absorption peak ($\hbar\omega_{\text{nir}} = E_{\text{HH}}$).

Figure 2 provides a representative sample of the observed NIR sidebands at 8.5 T. The thin lines represent the NIR signal while FIR radiation is on the sample, while the thick lines were obtained in the absence of FIR irradiation. Figure 2(a) shows both the up-converted ($\omega_{\text{nir}} + 2\omega_{\text{fir}}$) and down-converted ($\omega_{\text{nir}} - 2\omega_{\text{fir}}$) sidebands for a fixed NIR frequency of 12888 cm^{-1} and FIR frequency of 115 cm^{-1} . Note the greater intensity of the down-converted sideband at 12658 cm^{-1} compared to the up-converted sideband at 13118 cm^{-1} . This enhancement occurs as either $\hbar\omega_{\text{nir}}$ or $\hbar\omega_{\text{sideband}}$ approach E_{HH} . The broad background on the down-converted sideband is PL, enhanced due to carrier heating.⁹ Figure 2(b) shows the down-converted sideband at a FIR frequency of 103 cm^{-1} . The PL can be seen clearly, and the small enhancement of the high energy PL tail again is due to heating carriers with FIR radiation.⁹ The intensity of the sideband is several times greater than the PL amplitude, and the linewidth of the sideband is limited by the resolution of the monochromator (2 cm^{-1}). Figure 2(c) shows an up-converted sideband at a FIR frequency of 115 cm^{-1} . This sideband energy is far above the energy of radiatively recombining electrons and holes, so there is no PL background.

The intensity of the sideband radiation depends in a complicated fashion on the FIR frequency, NIR frequency, magnetic field, NIR intensity, and FIR intensity. We give here only a rough account of these dependences. Further details are reported in Ref. 15. Sidebands were observed only when both ω_{nir} and ω_{sideband} were in a region of nonzero NIR absorption. For example, no sidebands are observed when ω_{nir} is in the band gap or when ω_{sideband} is in the gap between the $1s$ HH excitonic absorption and the free-electron and heavy hole continuum. The sideband intensity is greatly enhanced when the magnetic field tunes the free-electron cyclotron frequency¹⁶ ω_{cr} near to ω_{fir} , as shown in Fig. 3 for fixed ω_{fir} and ω_{nir} . The frequency at which the sideband intensity is maximum as a function of magnetic field is shown in Fig. 4.¹⁷ Figures 3 and 4 indicate that, for fixed magnetic field, ω_{cr} is slightly higher than the frequency at which the intensity of the sideband is maximum. The intensity of the sidebands increases quadratically with increasing

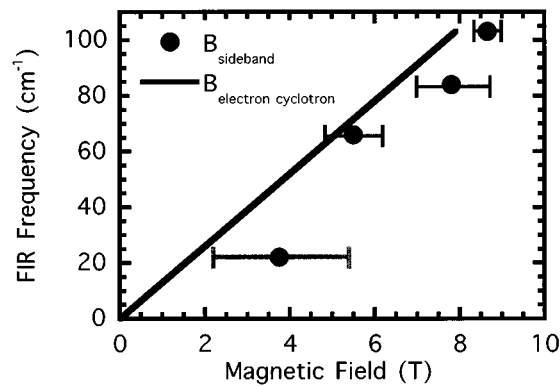


FIG. 4. Sideband generation resonance frequency as a function of magnetic field. The resonance frequency is close to, but consistently lower than the electron cyclotron resonance frequency.

FIR intensity over the full measurement range (up to several 100 kW/cm^2). The intensity of the sidebands increases linearly with increasing NIR intensity up to an intensity on the order of 500 mW/cm^2 , and then varies sublinearly.

We attribute the observed two-photon sidebands to resonantly enhanced four-wave mixing in which two FIR photons and one NIR photon mix to generate a NIR sideband photon. In time-dependent perturbation theory, the intensities of sidebands can be described by a third-order susceptibility $\chi^{(3)}$. Such a perturbative treatment predicts that the intensity of sidebands increases quadratically (linearly) with incident FIR (NIR) intensity, consistent with the dependence that we have observed. For NIR intensities greater than 500 mW/cm^2 , $\chi^{(3)}$ apparently saturates. The peak in the intensity of sidebands in Fig. 3, and the fact that sidebands are detected only when the linear absorption at ω_{nir} is nonzero, indicate that sidebands reported here occur only when $\chi^{(3)}$ is resonantly enhanced.

The phenomena reported here appear to be rather different than free-carrier-induced $\chi^{(3)}$ in semiconductors. Such third-order nonlinearities were first studied more than 30 years ago near $10 \mu\text{m}$ wavelength,¹⁸ and more recently in the FIR.^{3,19} Typically, such studies were performed on degenerately doped semiconductors, and are well-described by models in which parameters in the plasma dielectric function depend on light intensities.²⁰ Such a model appears not to be useful here, since the system is undoped and magneto-excitonic resonances are prominent. A detailed theoretical analysis of the experimental results presented here is in progress.

One-photon sidebands, which would be associated with a $\chi^{(2)}$ process, are not observed in this experiment. Bulk GaAs does have a nonzero $\chi^{(2)}$ due to a microscopic lack of inversion symmetry. However, this $\chi^{(2)}$ effect can only be excited with crossed FIR-NIR linear polarizations, which would result in a generated beam propagating perpendicular to the pumping beams. As a result, one does not expect to observe one-photon sidebands with the current experimental geometry.

We note that, in this experiment, the collected sideband emission propagates in a direction opposite to the incident NIR radiation. Phase-matching considerations strongly favor forward propagation of sideband radiation, but this is absorbed by the substrate in this experiment. Either the detected sideband radiation was reflected by the substrate, or phase-matching requirements were relaxed because the nonlinear interaction occurred in two dimensional QWs.

These results show that mixing between NIR and intense FIR radiation can dominate the NIR emission from GaAs/AlGaAs QWs. Possible applications include the conversion of FIR photons into distinct NIR photons for fast detection, terahertz frequency modulation of NIR radiation using FIR radiation for communication, and the study of FIR resonances in semiconductors using a novel nonlinear detection technique.

The authors gratefully acknowledge the discussions with H. Sakaki, S. J. Allen, Jr., A. G. Markelz, and A. Imamoglu. The authors would like to thank D. P. Enyeart and J. R. Allen at the Center for Terahertz Science and Technology for their technical support. This work has been supported by the NSF Science and Technology Center for Quantized Electronic Structures No. DMR 91-20007, JSTC Quantum Transition Project, ONR No. N00014-K-0692, and AFOSR No. F 49620-94-1-0158.

¹In many cases, the energy associated with the FIR electric field coupling to a dipole transition is comparable to both the transition and FIR photon energies.

²J. N. Heyman *et al.*, Phys. Rev. Lett. **72**, 2183 (1994).

³A. Markelz *et al.*, Semicond. Sci. Technol. **9**, 634 (1994).

⁴K. Craig *et al.*, Semicond. Sci. Technol. **9**, 627 (1994).

⁵B. Birnir *et al.*, Phys. Rev. B **47**, 6795 (1993).

⁶M. S. Sherwin, in *Quantum Chaos*, edited by G. Casati and B. V. Chirikov (Cambridge University Press, Cambridge, in press).

⁷J. Cerne *et al.*, Phys. Rev. Lett. **77**, 1131 (1996).

⁸S. M. Quinlan *et al.*, Phys. Rev. B **45**, 9428 (1992).

⁹J. Cerne *et al.*, Phys. Rev. B **51**, (1995).

¹⁰Q. Wu and X. C. Zhang, Appl. Phys. Lett. **67**, 3252 (1995).

¹¹C. Sirtori *et al.*, Appl. Phys. Lett. **65**, 445 (1994).

¹²H. C. Chui *et al.*, Appl. Phys. Lett. **66**, 265 (1995).

¹³R. Paiella and K. J. Vahala, IEEE J. Quantum Electron. **32**, 721 (1996).

¹⁴See, for example, R. M. Hart *et al.*, Opt. Lett. **16**, 1511 (1991).

¹⁵J. Kono *et al.*, Proceedings of 12th International Conf. on the Application of High Magnetic Fields in Semiconductors Physics (1996) J. Kono *et al.*, *Proceedings of 23rd International Conference on the Physics of Semiconductors*, edited by M. Sheffler and R. Zimmermann (World Scientific, Singapore, 1996), p. 1911.

¹⁶The free-electron cyclotron resonance frequency has been optically detected in this sample, and found to agree well with theory (see Ref. 7).

¹⁷Since 44 cm^{-1} is smaller than the HH exciton binding energy, no sidebands were observed at $\omega_{\text{nir}} = 22 \text{ cm}^{-1}$ when ω_{nir} was tuned to the HH exciton $1s$ state. Therefore, the scan at 22 cm^{-1} involved a fixed ω_{nir} at 12660 cm^{-1} (above the HH exciton continuum). ω_{nir} was not shifted to accommodate the diamagnetic shift. The resonance at 22 cm^{-1} was much broader than at higher frequencies, as reflected in the large error bar.

¹⁸C. K. N. Patel, R. E. Slusher, and A. Fleury, Phys. Rev. Lett. **17**, 1011 (1966).

¹⁹A. Mayer and F. Keilmann, Phys. Rev. B **33**, 6954 (1986); **33**, 6962 (1986).

²⁰S. Y. Auyang and P. A. Wolff, J. Opt. Soc. Am. B **6**, 595 (1989).